Progress in Nuclear Energy 191 (2026) 106043

Contents lists available at ScienceDirect

Progress in Nuclear Energy

journal homepage: www.elsevier.com/locate/pnucene

Assessment and experimental validation of the new wall boiling heat transfer model under different boundary conditions

Xiang Zhang [a,*], Jie Wan [a,b], Nikolai Rensch [a], Xu Cheng [a]

[a] Institute for Applied Thermofluidics (IATF), Karlsruhe Institute of Technology (KIT), Kaiserstrasse 12, 76131, Karlsruhe, Germany
[b] Key Laboratory of Low-Grade Energy Utilization Technologies and Systems, Ministry of Education, Chongqing University, Chongqing, 400044, China

ARTICLE INFO

Keywords:
Flow boiling
Wall boiling heat transfer model
Model assessment
CFD

ABSTRACT

Flow boiling widely exists in industrial systems because of its high heat transfer capability. In the previous study, we proposed a new heat transfer model for wall boiling through mechanism analysis (Zhang et al., 2024). As a newly developed model, it is quite important to explore the impact of different boundary conditions on model performance to provide potential directions for further improvement. In this paper, a series of flow boiling experiments for R134a within a wide range of boundary conditions (q_w = 80–260 kW/m^2, G = 1000–2000 kg/(m^2·s), P = 11–17 bar, $\Delta T_{in,sub}$ = 19–38 K) were carried out in a 10 mm-diameter vertical tube, providing more than 900 data points. The developed wall boiling model was validated using these experimental data for R134a boiling, as well as referenced water boiling and n-Perfluorohexane boiling experimental data in both pipes and rectangle channels. According to the results, the mean relative error of the wall superheat between our experimental data and the model predictions is ±31.5 %. In addition, an analysis was conducted to examine the influence of different boundary conditions on the accuracy of the developed model. The reasons for the discrepancy of the calculated results were analyzed and further improvements should be considered in the model.

Nomenclature

$C_{p,l}$	specific heat capacity/J·kg^{-1}·K^{-1}	Greek letters	
D	diameter/m	α	volume fraction
F	enhancement factor	ρ	density/kg·m^{-3}
F_1	convective correction factor	λ	thermal conductivity/W·m^{-1}·K^{-1}
F_2	boiling correction factor	σ	surface tension/N·m^{-1}
F_A	factor of vapor area effect	μ	viscosity/kg·m^{-1}·s^{-1}
F_B	factor of boiling destructive effect		
G	mass flow rate/kg·m^{-2}·s^{-1}	Subscripts	
h	heat transfer coefficient/W·m^{-2}·K^{-1}	e	evaporation
h_{fg}	latent of vaporization/J·kg^{-1}	fc	liquid forced convection
I	current/A	i	inner
L	length/m	l	liquid
P	Pressure/bar	LB	superheated liquid to bubble
q	heat flux/W·m^{-2}	mac	macroscopic
q_b	heat flux for bubble growth/W·m^{-2}	mic	microscopic
Q	heat/W	nb	nucleate boiling
Q_L	heat loss/W	o	outer
R	radius/m	P	pool boiling
S	suppression factor	q	quenching
T	temperature/K	s	saturation
u_τ	shear velocity/m·s^{-1}	sub	subcooling
U	voltage/V	v	vapor
V	volume/m^3	w	wall
w_b	bubble growth velocity/m·s^{-1}	WL	wall to liquid
x_e	Equilibrium quality	WB	wall to bubble

(*continued on next column*)

(*continued*)

1. Introduction

Subcooled flow boiling plays an important role in many industry systems because of its high heat transfer coefficient. This process can be affected by multiple factors, including the working fluid, mass flow rate, heat flux, inlet subcooling, pressure and channel geometry. The complexity of the physical phenomena in subcooled flow boiling, including nucleation and bubble behaviors, presents significant challenges in predicting subcooled flow boiling phenomena.

With advancements in computer technology, researchers have conducted extensive studies using the CFD method in the field of thermal-

* Corresponding author.
E-mail address: xiang.zhang@kit.edu (X. Zhang).

https://doi.org/10.1016/j.pnucene.2025.106043
Received 20 March 2025; Received in revised form 15 August 2025; Accepted 7 September 2025
Available online 12 September 2025

hydraulics. The CFD approach is valuable for studying bubble behaviors that are challenging to capture experimentally (Khoshnevis et al., 2018) and allows for comprehensive research on a wider range of thermal-hydraulic and structural parameters (Liang et al., 2023). Therefore, CFD simulation plays an important role in predicting two-phase flow phenomena. Accurate simulation of the wall boiling heat transfer is one of the key factors determining the distribution of the two-phase flow field. In CFD calculations of flow boiling, the wall boiling heat transfer model describes the physical processes at the heated wall during phase change, allowing the analysis of mass and energy transport mechanisms. Currently, there are two methods for calculating wall heat transfer within the Eulerian two-fluid framework.

The RPI model is the most widely used in CFD simulation. Although it was originally developed based on pool boiling experiments, it has been validated for subcooled flow boiling conditions (Braz Filho et al., 2016; Liu et al., 2021). The total wall heat flux in RPI model is divided into three parts, including liquid convection term q_{fc}, evaporation term q_e and quenching term q_q:

$$q_w = q_{fc} + q_q + q_e \tag{1}$$

Furthermore, several modified wall boiling models have been proposed based on the original RPI model and the analysis of the flow boiling mechanism. For example, Sateesh et al. (2005) accounted for the influence of sliding bubbles by dividing the bubble influence area into regions affected by sliding and stationary bubbles, respectively. Wang et al. (2022) proposed a modified wall boiling model for the subcooled flow boiling in a proposed a modified wall boiling model. Zhou et al. (2021) improved the RPI model by considering the condensation occurring at the top of the bubbles in subcooled flow boiling. However, several bubble dynamic parameters, such as active nucleate site density and bubble departure frequency, along with their related sub-models, present significant challenges in terms of convergence during numerical simulations (Yang et al., 2023). Besides, the accuracy of the simulations is dependent on the closure models related to these microscopic parameters.

The other popular model for wall boiling heat transfer is proposed by Chen (1966), which conceptualizes the total wall heat flux as the sum of two distinct mechanisms:

$$q_w = F \cdot q_{mac} + S \cdot q_{mic} \tag{2}$$

where q_{mac} and q_{mic} are macroscopic and microscopic heat flux, attributed to forced convection and boiling, respectively. An enhancement factor F was introduced to account for the impact of bubble-induced disturbances on heat transfer. Meanwhile, a suppression factor S was employed to capture the characteristics of the thermal layer under subcooled boiling conditions. Chen (1966) fitted the enhancement and suppression factors by experimental data by using the bulk flow parameters. Many researchers have explored the enhancement and suppression factors to develop corresponding correlations (Feldman et al., 2000; Orian et al., 2010). However, the application of the Chen correlation in 3D CFD simulations faces difficulties, primarily because the bulk flow parameters cannot be directly obtained from CFD simulations.

In summary, the existing modeling approach for wall boiling in CFD simulations requires further development. Therefore, a research project was initiated several years ago and is ongoing at the Institute of Applied Thermofluidocs (IATF) of the Karlsruhe Institute of Technology (KIT) to develop a new partitioning heat transfer model for CFD applications and to enhance the understanding of important boiling phenomena. In our previous study (Zhang et al., 2024), a new CFD modeling approach for the heat transfer in wall boiling was developed for CFD calculations, and preliminary validation was performed. Different from the RPI model, which relies on multiple parameters characterizing bubble dynamics, the new model depends on cell-scale macroscopic variables and local physical properties, aiming to improve computational stability. It has been preliminary validated in our previous works by using several different public experiments. However, the available experiment conditions were limited, making it difficult to isolate the effect of each boundary condition. Given the limitations of the reference data in our previous work, analyzing how different boundary conditions affect the results of the new model will be problem.

It is worth noting that varying boundary conditions may influence the performance of the new model due to some key sub-parameters. The assessments of the impact of different conditions on the model is an important part in the model development, which can provide suggestions for further model improvement. For example, the nucleate boiling factor F_2 in the new model, which considers the correction of boiling heat flux and was derived from bubble growth mechanisms, may be significantly affected by pressure. Similarly, mass flux has impacts on the bubble growth process and also influences the structure of the thermal boundary layer. Additionally, since bubble growth can destroy the thermal boundary layer, the convective correction factor F_1, which accounts for the effects of bubble influenced area and bubble disturbance, may be influenced by mass flux. Therefore, it is necessary to conduct more experiments under different boundary conditions and assess how these boundary conditions affect the accuracy and applicability of the proposed model.

In this study, a series of experiments using R134a were conducted in a vertical tube under different boundary conditions. Together with further experimental data bases from the open literature, a relatively wide range assessment for the new wall boiling model was performed for both R134a boiling, water boiling and n-Perfluorohexane boiling in vertical pipes and rectangle channels. Based on the established database, the impacts associated with boundary conditions on the performance of the new model were investigated.

2. Mathematical models

2.1. Wall boiling heat transfer model

In earlier research, we has proposed a novel approach for modeling wall boiling heat transfer (Zhang et al., 2024). The key characteristics of the proposed model will be briefly summarized in present study.

According to the new boiling heat transfer model, as shown in Fig. 1, the total heat transferred from the heated wall consists of two parts. On the one hand, energy transport occurs from the heated surface into the microlayer beneath the vapor bubble, which contributes to the bubble growth (Q_{WB}) and it is assumed to be consistent with that in a saturated pool boiling in this study, i.e. $Q_{WB} = Q_{WB,P}$. On the other hand, the heat is transferred from the wall to the superheated layer denoted as Q_{WL}. The total wall heat can be written as:

$$Q_{total} = Q_{WL} + Q_{WB} \tag{3}$$

Therefore, the wall heat flux q_w can be written as a combination of forced convection contribution q_{fc} and nucleate boiling contribution q_{nb}, each adjusted by empirical correction coefficients:

$$q_w = F_1 \cdot q_{fc} + F_2 \cdot q_{nb} \tag{4}$$

where F_1 and F_2 are convective correction factor and boiling correction factor, respectively.

2.1.1. Liquid convective contribution

The convective contribution to the wall heat flux is calculated as:

$$q_{fc} = h_{fc} \cdot (T_w - T_l) \tag{5}$$

where T_w and T_l are wall temperature and liquid temperature, respectively. The convective heat transfer coefficient for liquid h_{fc} can be obtained from the wall function approach used in CFD simulations (Lin et al., 2021).

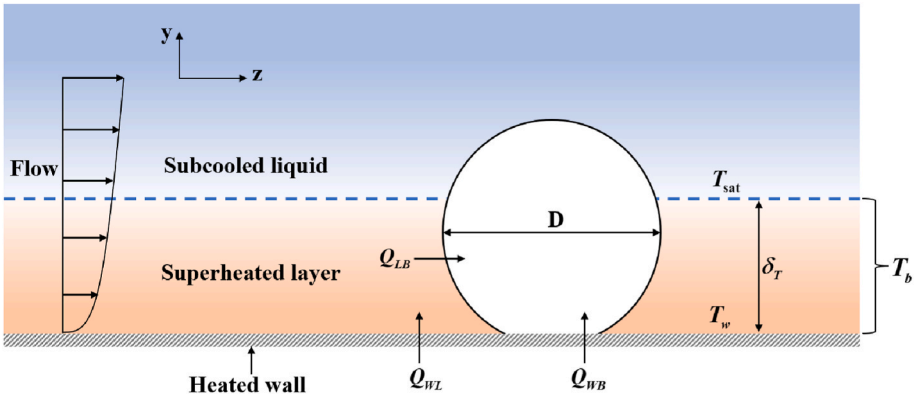

Fig. 1. Heat transfer during bubble growth.

2.1.2. Correction coefficient for liquid convective

The coefficient of the liquid convective heat transfer is influenced by the bubble dynamics in the process of wall boiling. Accordingly, a convective correction factor is introduced by considering two effects.

1) The area covered by bubbles on the heated wall should be excluded, which is expressed by a factor of F_A.
2) Bubble dynamic behaviors, including growth and lift, disrupt the near-wall thermal boundary layer, thereby enhancing the liquid convective heat transfer, as captured by the factor F_B.

The liquid convective correction factor F_1 can be written as:

$$F_1 = F_A \cdot F_B \tag{6}$$

The effect of the bubble influenced area is quantified by considering the local vapor volume fraction within the first grid layer:

$$F_A = 1 - \alpha_v \tag{7}$$

The enhancement factor F_B, influenced by bubble dynamics, is simplified as:

$$F_B = 1 + C_1 \frac{w_b}{u_\tau} = 1 + C_1 \frac{q_b}{h_{fg}\rho_v}\sqrt{\frac{\rho_l}{\tau_w}} \tag{8}$$

where w_b, q_b, h_{fg}, u_τ and τ_w, are the bubble growth velocity, heat flux associated with bubble growth on the wall, latent of vaporization, liquid shear velocity and wall shear stress, respectively. C_1 is an assumed coefficient (Zhang et al., 2024).

2.1.3. Nucleate boiling contribution

According to the formulation proposed by Forster and Zuber (1955), the contribution of nucleate boiling heat flux is expressed as:

$$q_{nb} = h_{nb} \cdot (T_w - T_s) \tag{9}$$

$$h_{nb} = 0.00122 \frac{\lambda_l^{0.79} C_{p,l}^{0.45} \rho_l^{0.49}}{\sigma^{0.5} \mu_l^{0.29} h_{fg}^{0.24} \rho_v^{0.24}} (T_w - T_s)^{0.24} (P_w - P_s)^{0.75} \tag{10}$$

2.1.4. Correction coefficient for boiling

However, the nucleate boiling heat flux, as determined by Eq. (10), which theoretically includes both the liquid convective part and nucleate boiling part in pool boiling (Forster and Zuber, 1955). Therefore, the pool boiling liquid convective part should be excluded from Eq. (10). In the proposed model for wall boiling, a correction coefficient F_2 is characterized by the fraction of nucleate boiling heat within the total heat transfer:

$$F_2 = \frac{Q_{WB,P}}{Q_{WL,P} + Q_{WB,P}} = \frac{1}{1 + \frac{Q_{WL,P}}{Q_{WB,P}}} \tag{11}$$

Finally, the boiling correction factor was obtained based on bubble growth dynamics and is expressed by the following equation (Zhang et al., 2024):

$$F_2 = \frac{1}{1 + \left(\sqrt{2} \cdot C_2 \cdot \frac{1-\alpha_v}{\alpha_v} \cdot \frac{B_{LB}}{B_{WB}^2 \cdot B_{WB}} \cdot \frac{\rho_v h_{fg}}{\rho_l C_{p,l}}\right)^{0.5} \cdot \left(\frac{1}{T_w - T_s}\right)^{0.5}} \tag{12}$$

2.2. Auxiliary models to close two-fluid model

The new wall boiling heat transfer model has been implemented into the two-fluid framework in ANSYS-Fluent by using the User Defined Function (UDF). The phase interactions can be realized through the interfacial transfer terms, which can be determined by the closure models summarized in Table 1.

3. Experimental measurements

3.1. Experimental facility

The experimental facility of KIMOF, developed at our institute, has been employed to investigate post-dryout heat transfer phenomena by Köckert et al. (2021). We attempted to select some useful results from the post-dryout experiments to preliminarily validate the model in our earlier study (Zhang et al., 2024). However, since the old experiments were mainly conducted for post-dryout, the available wall boiling data were limited, making it difficult to isolate the effect of each boundary condition. This complexity makes it challenging to assess the impacts associated with boundary conditions on the performance of the new

Table 1
Closure models for simulation.

Parameters	Model
Wall boiling heat transfer	New wall boiling heat transfer model (Zhang et al., 2024)
Turbulence	Standard k-ε model (Zhang et al., 2015)
Turbulence interaction	Sato model (Sato and Sekoguchi, 1975)
Interfacial transfer	
Interfacial area concentration	Symmetric model (ANSYS-Fluent, 2011)
Bubble diameter	Improved Unal model (ANSYS-Fluent, 2011)
Drag force	Ishii model (Ishii, 1990)
Lift force	Moraga model (Moraga et al., 1999)
Wall lubrication force	None
Turbulent dispersion force	Lopez-de-Bertodano model (de Bertodano, 1992)
Liquid-interface heat transfer	Ranz-Marshall model (Ranz, 1952)
Vapor-interface heat transfer	Lavieville et al. model (Lavieville et al., 2005)
Interfacial mass transfer	Energy balance

model using the reference data from our previous works.

As a part of our research project, the test section of KIMOF was renewed in this study, and a series of experiments were conducted to generate additional experimental data for assessing our wall boiling heat transfer model. The structure of KIMOF loop has been shown by Köckert et al. (2021). The working fluid for the system was R-134 refrigerant, which was circulated through the main loop by a coolant pump. The fluid first flows through a preheater, where it is heated up to a stable inlet temperature before entering the test section. After flowing through the test section, the refrigerant R-134 was cooled by a cooling tower and a cooling machine. The mass flux and the outer wall temperature of the test section are measured using a Coriolis mass flow meter and T-type thermocouples, respectively. The system pressure was controlled using a pressurizer that operates with hydraulic oil. The measurement uncertainties for temperature, mass flow rate, and pressure were 1 °C, 0.15 % and 0.25 %, respectively. All measurement parameters were displayed and saved by the LabVIEW software.

The test section was a tube, 1 m in length with a 10 mm inner diameter, as presented in Fig. 2(a) and (b). The application of thermal insulation allowed the surface to be approximated as adiabatic. Heating was provided by two current connectors. The working fluid flowed in an upward direction. There were 20 measuring locations along the test section, with a longitudinal distance of 60 mm or 30 mm between adjacent locations. At some locations, two thermocouples were symmetrically distributed around the circumference of the test section. A total of 24 thermocouples were installed along the test section to monitor the outer wall temperature.

3.2. Data reduction

Flow boiling tests were conducted under steady-state conditions. More than 40 sets of experiments were performed under different boundary conditions, such as pressure and mass flux, following to the single variable principle. The range of experimental conditions is summarized in Table 2.

The average heat flux q_{ave} can be calculated:

$$q_{ave} = \frac{UI - Q_L}{\pi L_H D_i} \tag{13}$$

where U, I, Q_L, L_H, D_i are the voltage, current, heat loss, heated length and inner diameter, respectively.

The inner wall temperature is determined from the measured outer wall temperature using the following equation:

$$T_{w,i} = T_{w,o} - \left(\frac{q_V}{16k}\right)\left(D_i^2 - D_o^2\right) + \frac{D_o}{2k}\left[\left(\frac{q_V D_o}{4} - q_L\right)\log\left(\frac{D_i}{D_o}\right)\right] \tag{14}$$

$$q_V = \frac{UI}{\frac{\pi}{4}L_H\left(D_o^2 - D_i^2\right)} \tag{15}$$

$$q_L = \frac{Q_L}{\pi L_H D_o} \tag{16}$$

where $T_{w,i}$, $T_{w,o}$, D_o, k, q_V and q_L denote the inner and outer wall temperature, inner diameter of the tube, thermal conductivity, volumetric heat flux and heat loss at the outer wall, respectively.

Table 2
Experimental conditions.

	IATF (2024)	Wang et al. (2022)	Devahdhanush et al. (2022)	Bartolemei et al. (1982)
Fluid	R134a	Water	n-Perfluorohexane	Water
Channel	Pipe	Rectangle	Rectangle	Pipe
Pressure [bar]	11–17	11–40	1.3–1.6	30–150
Mass flow rate [kg/(m^2·s)]	1000–2000	267	2400–3200	405–2123
Wall heat flux [kW/m^2]	80–260	123–163	138–386	420–2210
Inlet subcooling [K]	19–38	48–74	6	12–143
Experimental data	T_w	T_w	T_w	α_v

4. Results and discussion

4.1. Model performance

To evaluate the performance of the new wall boiling heat transfer model across different fluids and channel geometries, in addition to our wide range experimental database for R134a, we also employed data from the Wang experiments (Wang et al., 2022) on water boiling in a vertical rectangular channel, Bartolemei experiments (Bartolemei et al., 1982) on water boiling in a vertical pipe, and Devahdhanush

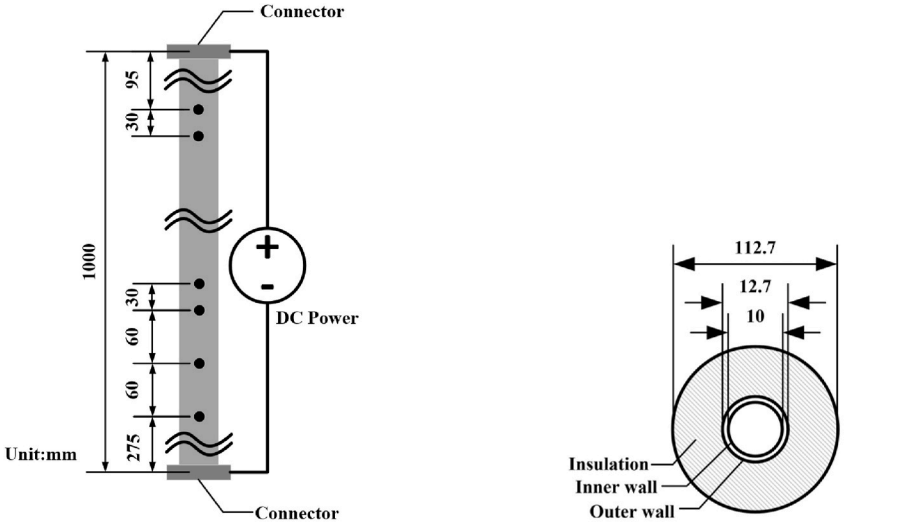

(a) Axial of the test section (b) Cross-section of the test section

Fig. 2. Test section of KIT Model Fluid Facility (KIMOF).

experiments (Devahdhanush et al., 2022) on n-Perfluorohexane boiling in a vertical rectangular channel, as summarized in Table 2. The wall superheat was selected as the primary parameter for comparison with experimental data, consistent with other studies on wall boiling models (Gilman, 2014; Shi et al., 2020). It is because that, for a given total wall heat flux, the wall boiling heat transfer model directly impacts the results of wall temperature. Additionally, the database of void fraction was also used in this work to further validate the model performance, because the evaporation heat flux on heated wall significantly contributed to vapor generation.

4.1.1. Wall temperature

(1) IATF experiment (R134a boiling)

The experiments of flow boiling in a vertical pipe were performed on KIMOF in IATF, as introduced in Section 3, and wall boiling heat transfer characteristics were studied. The wall boiling heat transfer model as well as the models introduced in Section 2 will be applied to the simulation of over 40 experimental cases. In simulations, a 2-D axisymmetric geometry is utilized to simplify the analysis of the fluid domain, which consists of a circular tube with a diameter of 10 mm and a length of 1 m, as illustrated in Fig. 3. A constant heat flux is applied to the tube wall to induce heating.

To achieve a grid independent solution, four sets of meshes with different numbers of nodes were tested in the axial and radial directions, as summarized in Table 3. The simulations were conducted under the conditions of $P = 11$ bar, $G = 2000$ kg/(m^2·s), $\Delta T_{\mathrm{in,sub}} = 38$ K, and $q_w = 260$ kW/m^2. Since the standard k-ε turbulence model with wall functions was employed, it is essential to ensure that the first-layer mesh cells don't fall within the viscous sublayer. Based on the results shown in Fig. 4, Mesh 2 was selected for this study, as it ensured that the y + values in the near-wall cells exceeded 30.

In our experiments, more than 900 data points have been collected, providing a comprehensive database for evaluating the model's performance. The wall superheat predicted by the new model is compared with experimental data under the conditions of $q_w = 80$–220 kW/m^2, $P = 11$–17 bar, $\Delta T_{\mathrm{in,sub}} = 19$–$38$ K, $G = 1000$–2000 kg/(m^2·s), as illustrated in Fig. 5(a). The results show that the total Mean Relative Error (MRE) between the calculated and measured values is 31.5 %, which is determined by the following equation:

$$MRE = \frac{1}{n}\sum_{i=1}^{n}\left|\frac{\Delta T_{w,cal,i} - \Delta T_{w,\exp,i}}{\Delta T_{w,\exp,i}}\right| \times 100\% \tag{17}$$

It's worth noting that the MRE of ±31.5 % is still a substantial error, however, for flow boiling, where the strong coupling of phase change and interphase interactions makes accurate prediction challenging, such an error for the preliminary version of model is within the range generally considered acceptable. Since the RPI fails to obtain a converged solution using the same combinations of sub-models in some working conditions, such as high quality, it shows the potential advantage of the new model in computational stability. Fig. 5(b), (c), and (d) depict the MREs calculated under different pressure, mass flux, and inlet subcooling, respectively. The results indicate that except for the cases under $P = 17$ bar, the MREs remain within 50 % under most other conditions. Pressure exhibits a significant impact on the MREs of the new model's predictions. Specifically, when pressure increases to 17 bar, the performance of the new model becomes very poor, yielding an MRE of 141.0 %. Under high mass flux or high inlet subcooling conditions, the model generally predicts a lower wall temperature compared to the experimental values when the wall superheat is low. Even in cases where some measured wall temperatures exceed the saturated temperature, the wall temperature calculated by the model is still lower than the saturated temperature. This discrepancy may be caused by an overestimation of the convective heat transfer coefficient for the subcooled liquid. A detailed discussion of the effects of pressure, mass flux, and inlet subcooling on the model's performance will be presented in the following section.

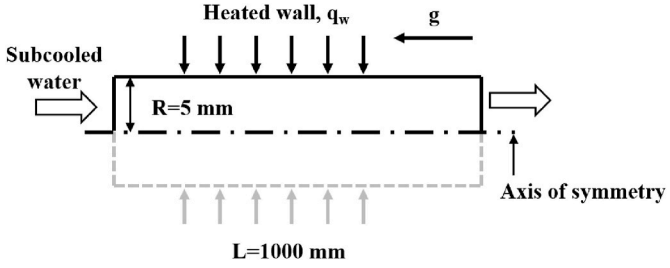

Fig. 3. Simulation domain of IATF experiment.

Table 3
Mesh information of IATF experiment.

No.	Radial nodes	Axial nodes
Mesh1	30	1000
Mesh2	35	1000
Mesh3	35	2000
Mesh4	40	1000

(2) Wang experiment (water boiling)

Besides utilizing our experimental data for R134a boiling from IATF, we also tested the new model against water boiling experiments from Wang et al. (2022). A vertical upward rectangular channel (50 mm high, 2.5 mm wide) with a heating section of 0.8 m was used in the experiment. The boundary condition ranges are summarized in Table 2. Following a similar mesh sensitivity analysis as before, a 3D rectangular channel was established with 6 grids in width, 60 grids in height, and 200 grids in length. Fig. 6 presents a comparation of the wall superheat calculated using the new model, as well as traditional RPI model, and experimental data along centerline for four different cases. In the two-phase boiling region, the new model's calculated wall superheat for case No.627 agrees well with the experimental data. However, for the other cases, both the new model and the RPI model underestimated the wall superheat is, suggesting that the heat transfer coefficient in boiling region is underestimated under these conditions. A deviation is observed in the calculated wall temperature slope in the single-phase region compared to the experimental data. This phenomenon was also reported by Wang et al. (2022), where it was explained by the reason that the unsteady experimental heating efficiency caused an error in the values of wall heat flux.

(3) Devahdhanush experiment (n-Perfluorohexane boiling)

The flow boiling experiments conducted by Devahdhanush et al. (2022) was also employed in this work to evaluate the new model's performance for n-Perfluorohexane boiling. It was conducted in a vertical upward rectangular channel with an upstream development length of 0.3277 m and a heating length of 0.1146 m. The width between the heated wall and the side wall was 2.5 mm and the height between the other unheated wall was 5 mm. The boundary conditions with single-sided heating are summarized in Table 2. Following a similar mesh sensitivity analysis as before, a 3D rectangular channel was established with 11 grids in width, 20 grids in height, and 350 grids in length. Fig. 7 presents a comparation of the calculated wall superheat and experimental data. It worth noting that the traditional RPI model significantly overpredicted the wall temperature, likely because its sub-models are not suitable for n-Perfluorohexane, thus the RPI results are not presented here. Fig. 7 shows that the model reasonably predicts the wall superheat for n-Perfluorohexane boiling under different heat

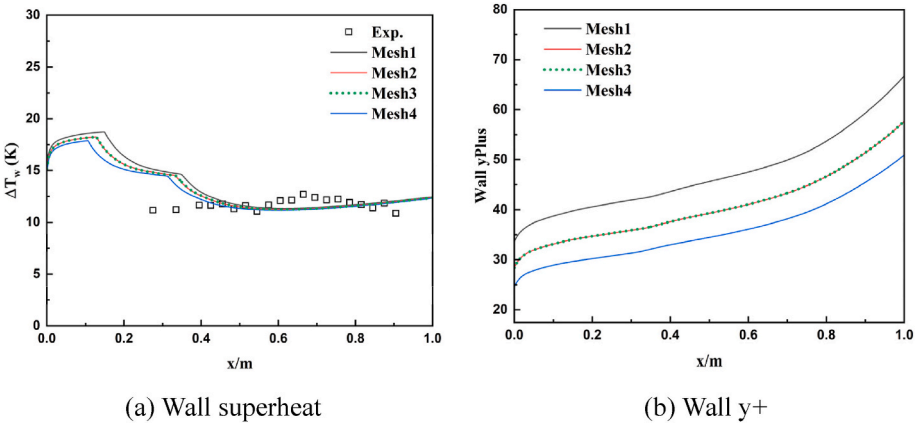

Fig. 4. Mesh sensitivity analysis of IATF experiment.

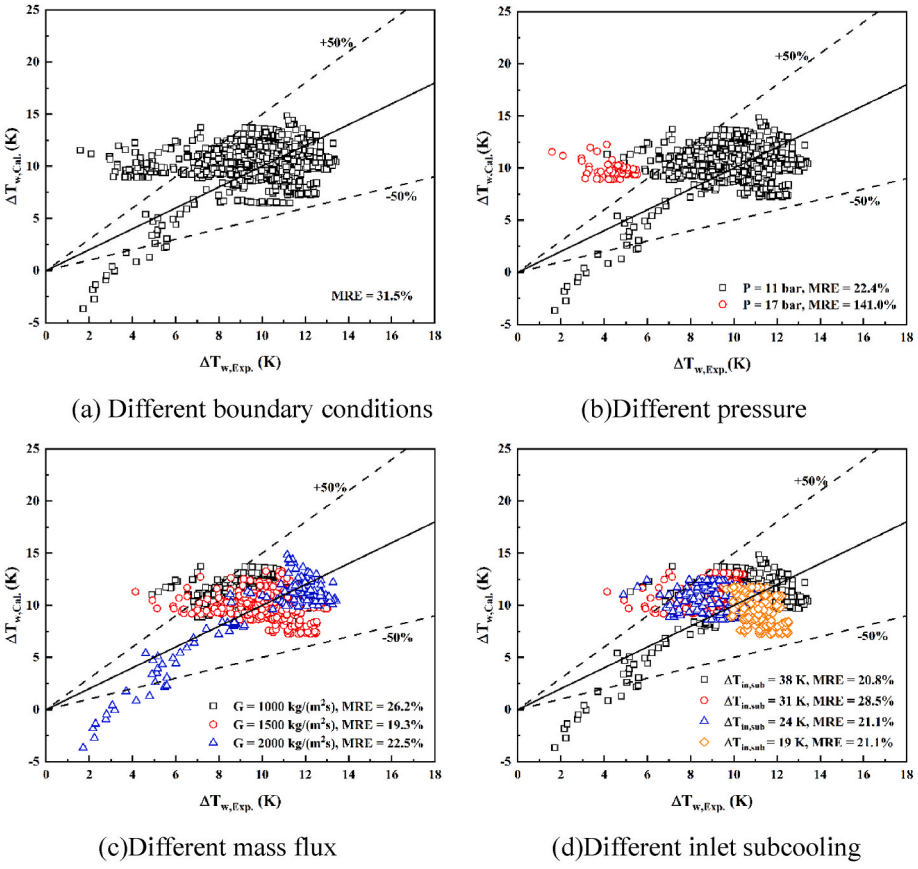

Fig. 5. Comparison of wall superheat between simulated and experimental results of IATF experiment.

flux. This shows that the new model has great potential not only in the calculation of water boiling and R134a boiling, but also has good performance in the calculation of n-Perfluorohexane boiling.

4.1.2. *Void fraction*

The limited experiment data published by Bartolemei and Chanturiya (1967) in 1967 have been employed in our earlier study (Zhang et al., 2024) for the preliminary validation of the new model. Bartolemei et al. (1982) later conducted a series of experiments in a vertical pipe with a diameter of 12 mm for water boiling and the data of cross-section average void fraction were published in 1982. Following a similar mesh sensitivity analysis as the simulation of IATF experiments, a 2-D axisymmetric geometry was employed with 40 grids in radius and 800 grids in length. Fig. 8 gives a comparation between the calculated void fraction and the experimental data provided by Bartolemei et al. (1982). The equilibrium quality was calculated based on energy balance. A vertical test section with a 12 mm diameter was used to conduct the experiments with water as the working fluid.

Fig. 8 shows the calculated void fraction are consistent with the experimental values in terms of overall trend. However, when the heat flux is high, as shown in Fig. 8(a), or the mass flow rate is low, as shown in Fig. 8(c), the cross-section average void fraction is underestimated in the regions with low equilibrium quality. This discrepancy may be attributed to the overestimation of the heat transfer capacity of the single-phase liquid by new model under subcooled boiling conditions. This overestimation could result in an underestimated boiling phase-

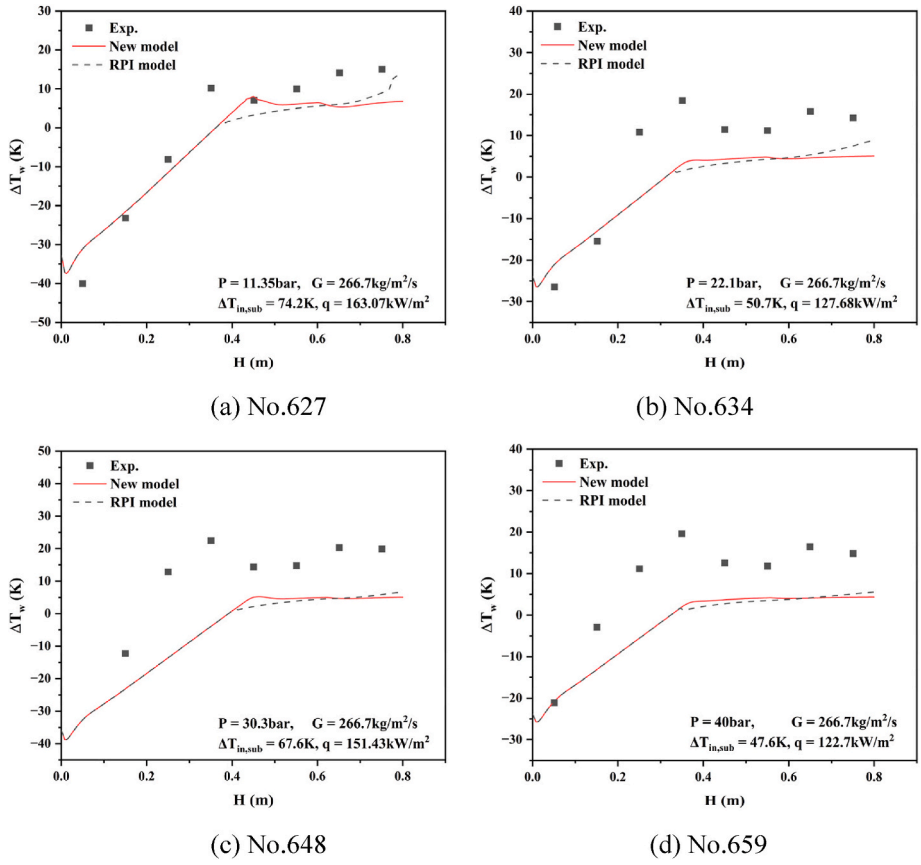

Fig. 6. Calculated wall superheat and experimental data of Wang experiment.

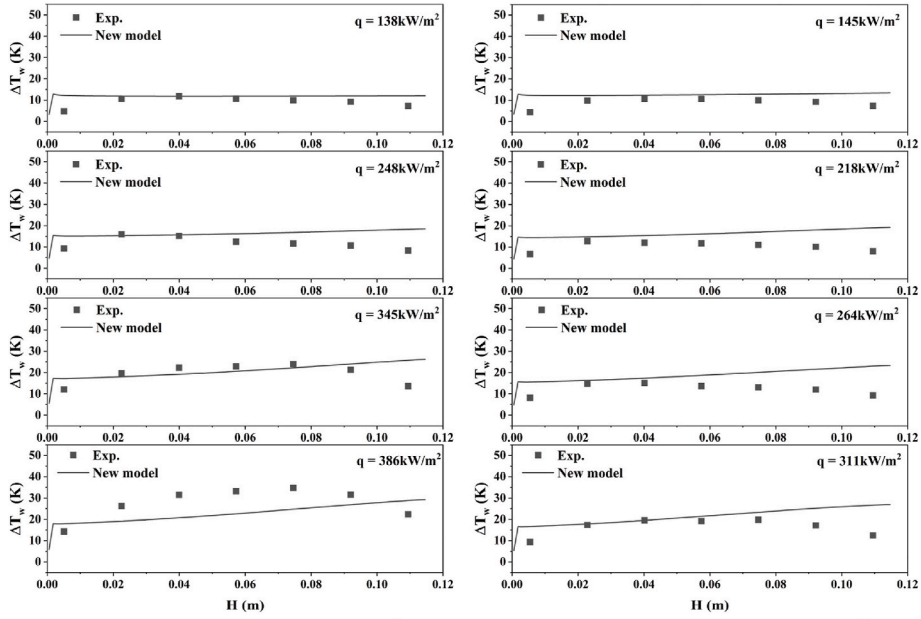

Fig. 7. Calculated wall superheat and experimental data of Devahdhanush experiment.

change heat flux, thereby leading to an underprediction of the void fraction. As the equilibrium quality increases with heating length, this deviation decreases. Another possible reason is the occurrence of subcooled boiling when equilibrium quality is negative, where the bulk liquid remains subcooled. Since the new model only focuses on wall heat transfer, the closure model listed in Table 1 account for interphase heat and mass transfer in the bulk region may has defects in the calculation of evaporation and condensation.

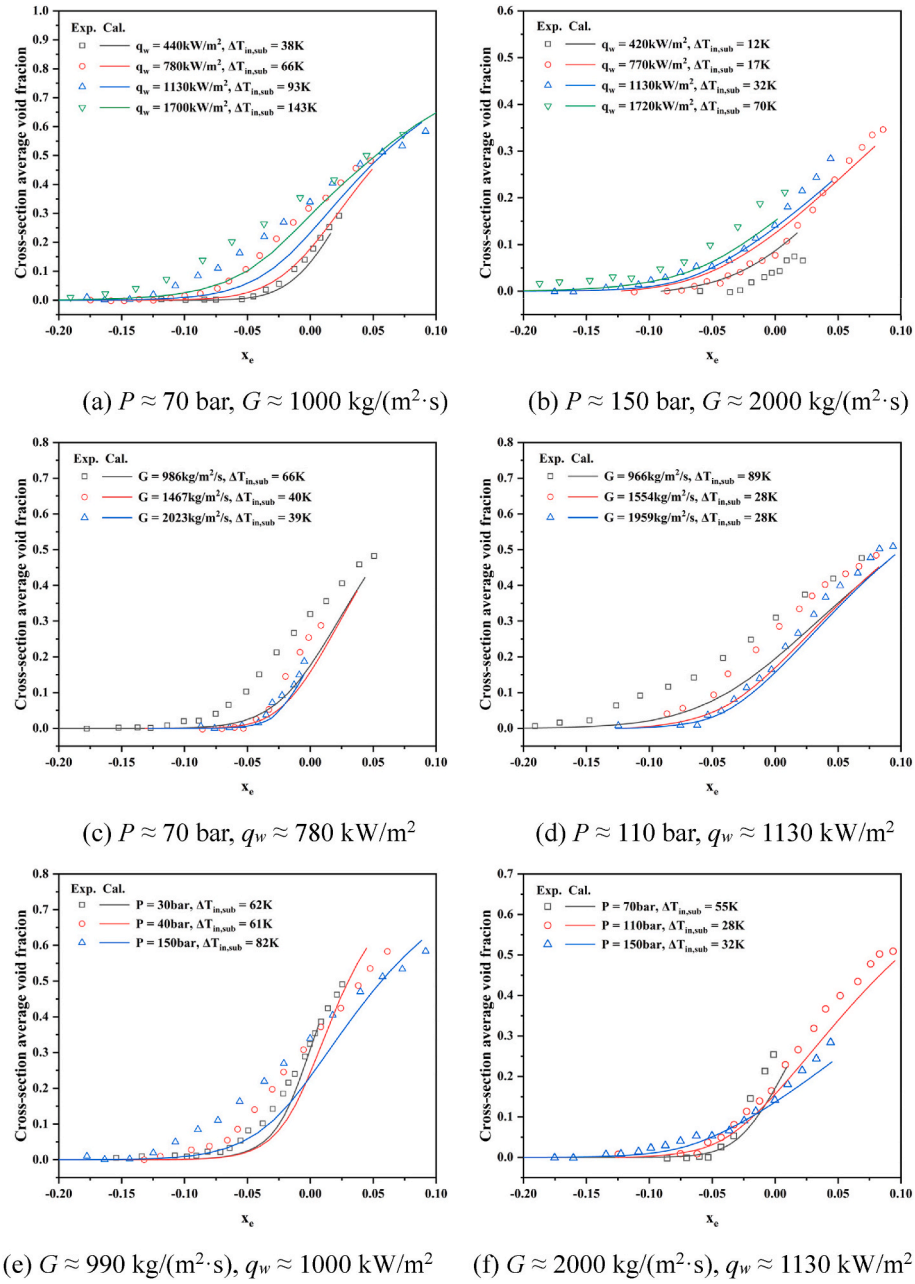

Fig. 8. Calculated cross-section average void fraction and experimental data of Bartolemei experiment.

Fig. 9 gives a comparation between the new model and the RPI model for the case in Bartolemei experiment. It can be seen that once x_e exceeds −0.05, the RPI model predicts an instantaneous increase in evaporative heat flux. Although the cross-section averaged void fraction predicted by the RPI model is slightly closer to the experimental data, this does not necessarily mean that the RPI model produces the correct distribution of evaporative heat flux. In the RPI model, the calculation of evaporative heat flux strongly depends on several bubble dynamic parameters, such as the nucleate site density and bubble departure frequency, each of which has large uncertainties. In our calculations, the nucleate site density in the RPI model was calculated using the empirical correlation proposed by Lemmert and Chawla (1977), which assumed that the nucleate site density depends only on the wall superheat in a power-law manner. As a result, when the wall temperature increases, it may cause the nucleate site density to grow rapidly, leading to a rapid rise in evaporative heat flux. Therefore, this rapid increase phenomenon in the RPI model may originate from the limitations of its sub-models and does not necessarily reflect the actual physical process.

Besides, Fig. 9 shows that the evaporative heat flux predicted by new model decreases when $-0.15 < x_e < -0.1$. This is because increasing bubble generation enhances the boiling disturbance effect on the liquid thermal layer. As shown in Fig. 10, in the range of $-0.15 < x_e < -0.1$, the convection enhancement factor F_1 increases significantly, causing the liquid convective heat flux to rise and leading to a decrease in evaporative heat flux. However, as boiling becomes more intense, the high efficiency of boiling heat transfer enables the evaporative heat flux to dominance.

4.2. *Entrance effects with different subcooling*

The analysis of the entrance effects with different subcooling was performed based on the simulations of IATF experiment. Fig. 11(a) shows the comparation between the calculated and measured wall superheat under different inlet subcooling. The results indicate that inlet

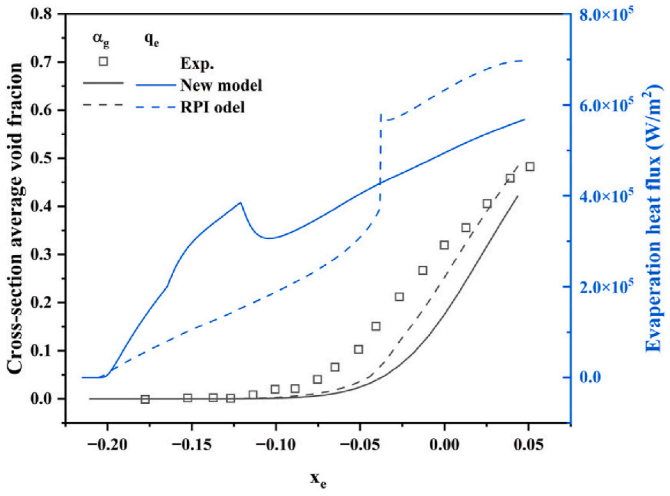

Fig. 9. Comparation results between the new model and RPI model ($P \approx 70$ bar, $q_w \approx 780$ kW/m^2, $G = 986$ kg/(m^2·s), $\Delta T_{in,sub} = 66$K).

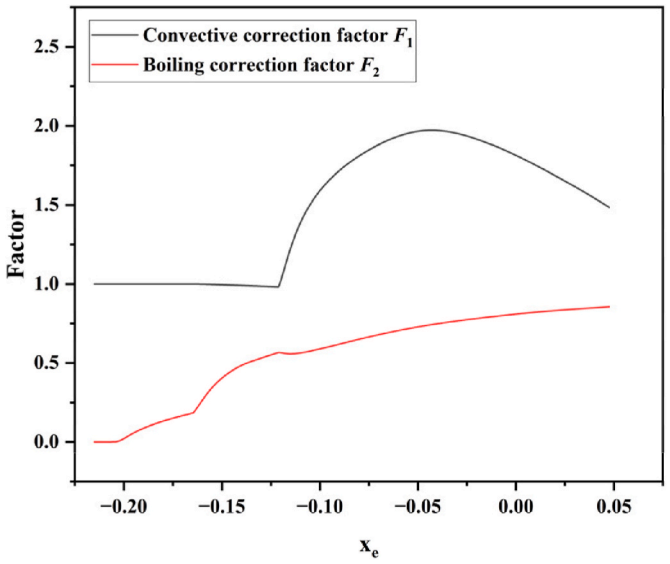

Fig. 10. Results of correction factors by new model.

subcooling primarily influences predicted wall temperature and heat flux in the inlet region due to the entrance effects.

It can be seen that the current model reasonably predicts the wall superheat with a slight overestimation in the fully-developed boiling region, but shows significant deviation near the inlet ($x_e < -0.2$), especially under high inlet subcooling conditions. First, this deviation may come from simplifying assumptions in the current model. For example, it assumes that the heat transferred from the heated surface into the microlayer beneath the vapor bubble, using for bubble growth, is consistent with that in a saturated pool boiling ($Q_{WB} = Q_{WB,P}$). This simplifying assumption may need further improvement when calculating subcooled boiling with high subcooling. Second, the new model may underestimate convective heat transfer. As shown in Fig. 12, at high subcooling, the liquid temperature in the first-layer grid is significantly higher than the bulk liquid temperature. Since Eq. (5) uses the first-layer temperature rather than the bulk temperature, this leads to underestimation of the convective heat transfer. In addition, the convective enhancement factor F_B in Eq. (8) is assumed to vary linearly with the ratio of bubble growth velocity to liquid shear velocity, with a constant coefficient C_1. The bubble growth velocity is calculated by the sum of evaporation effect and condensation effect. As shown in Fig. 11 (d), vapor appearance in the wall-adjacent cells is delayed with increasing inlet subcooling. Thus, under high subcooling, F_B may be underestimated due to condensation effect.

Besides, although the inlet temperatures differ among the three cases, as the equilibrium quality changes, when the equilibrium quality is larger than −0.05, the predicted wall superheat of the three cases is similar and significantly better than those conditions of lower equilibrium quality. These results suggest that the current new model may be insufficient in accurately predicting the transition from single-phase convection to saturated boiling under subcooled liquid conditions, and is more suitable for predicting fully-developed boiling.

4.3. Effects of mass flow rate

To study the effect of mass flow rate on model performance, a sensitivity analysis was conducted using the experimental database from IATF. Fig. 13(a) presents the calculated wall superheat and experimental data under different mass flow rate. From the experimental data, we can see that boiling occurred at the measurement locations of the three groups of experiments and the wall temperature remains a relatively stable value with fluctuations under different equilibrium quality, which may be caused by bubble departure or sliding behavior.

As shown in the calculated data in Fig. 13(a), in the boiling region, the predicted wall superheat is within the error range of the experimental value, indicating that the new model reasonably calculates the wall temperature under different mass flow rates. Near the inlet of the test section, the predicted wall superheat under higher mass flow rate is lower than that observed under other conditions due to the higher liquid convective heat flux. However, since heat transfer is dominated by convection at this stage, the wall temperature continues to increase. As boiling occurs (with the x_e around −0.38 for $G = 1000$ kg/(m^2·s)), the vapor appears in the first-layer grids, as shown in Fig. 13(d). At this stage, the contribution of boiling heat transfer increases, leading to a gradual decrease in wall temperature, as shown in Fig. 13(b). As evaporation increases the vapor generation rate, the convective heat transfer enhancement caused by bubble disturbance becomes more significant, as shown in Fig. 13(c) that F_1 rapidly increases, leading to a further reduction in wall temperature. For example, within $G = 1000$ kg/(m^2·s), this effect is observed at approximately $x_e = -0.25$. It worth noting that both bubble departure and sliding will disturb the thermal boundary layer, which are significantly affect by flow rate. However, these effects were not considered in the bubble disturbance term F_B of current new model, as shown in Eq. (8). It may underestimate the convective enhancement effect under different mass flow rate conditions.

4.4. Effects of pressure

To study the effects of pressure on model performance, a sensitivity analysis was conducted using the experimental database from IATF. Fig. 14(a) presents the predicted and experimental wall superheat at 11 bar and 17 bar, separately. The new model shows good agreement with the measured wall superheat at 11 bar. However, at 17 bar, the calculated wall superheat does not decrease as much as the experimental measurements, leading to an overestimation of wall temperature. It indicates that pressure has a significant impact on the performance of new model in current version and suggests that the current new model does not seem to accurately capture pressure effects.

This may be caused by the assumption that the bubble volume increases linearly with the volume contribution from microlayer evaporation, as described by Eq.(54) of Zhang et al. (2024). It is worth noting that pressure may have a significant influence on bubble growth rate and bubble size. For example, as reported by Dahariya and Betz (2019), bubble size was reduced by 46 % when pressure increased from atmospheric conditions to 6 bar, while Utaka et al. (2014) observed that, at bubble inception, microlayer evaporation could account for about 15 %–70 % of the total bubble volume, depending on the wall superheat. These

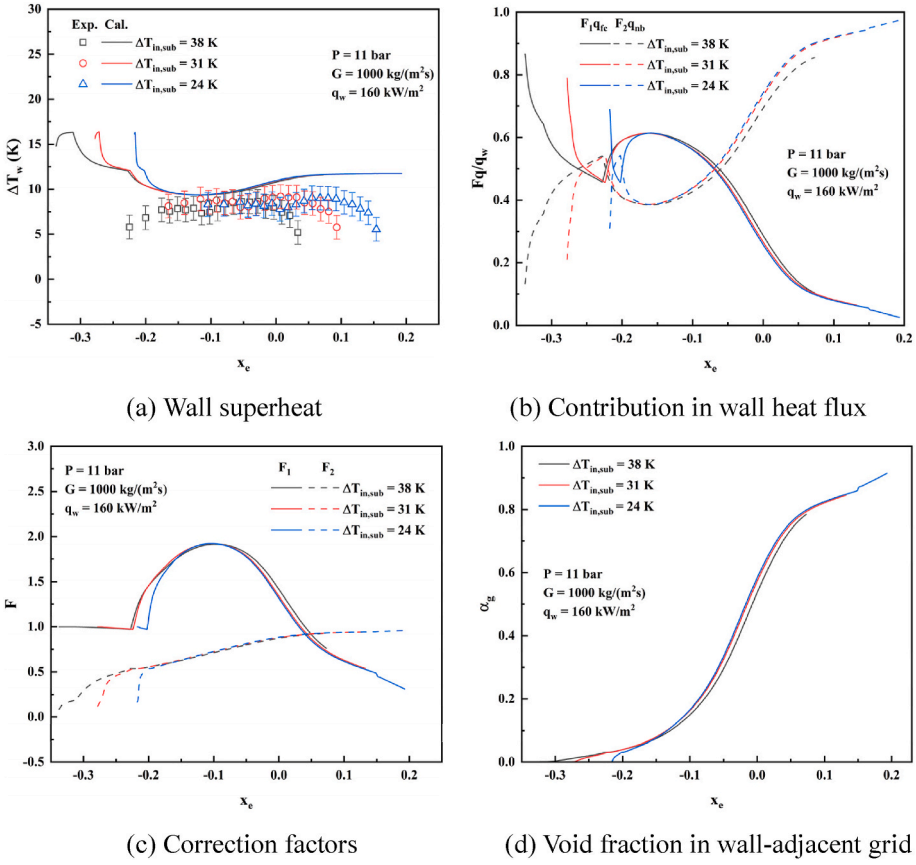

Fig. 11. Analysis of the entrance effects with different subcooling.

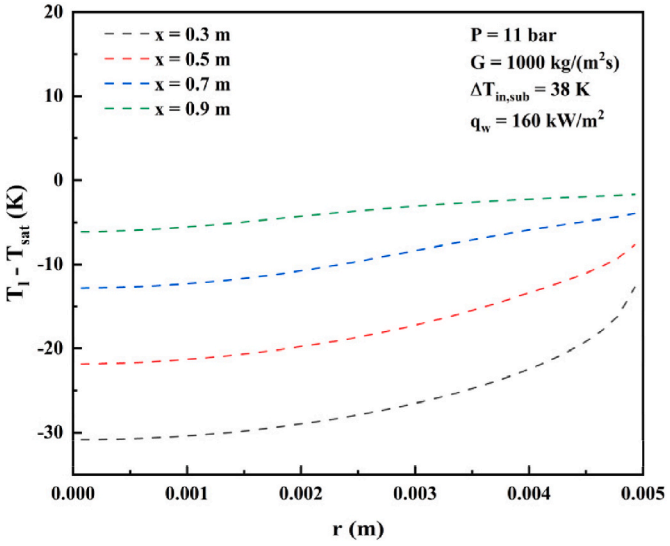

Fig. 12. Radial distribution of liquid subcooled temperature.

suggest that the coefficient C_G in Eq. (54) of Zhang et al. (2024) may be dependent on pressure and wall superheat rather than a constant. As shown in Fig. 14(b), due to the lack of consideration for pressure effects on bubble size, the nucleate boiling correction factor F_2 remains similar at 11 bar and 17 bar in the nucleate boiling region. As a result, when the heat transfer is dominated by nucleate boiling, the predicted wall temperatures cannot accurately capture variations under different pressures. In future works, a possible way to improve this model is to enhance the coefficient C_G by introducing parameters such as pressure and superheat, thereby relaxing the current linear assumption for the microlayer evaporation contribution to the total bubble volume.

The other aspect is that, in the current model, the enhancement of convective heat transfer is accounted for by an enhancement factor F_B, as shown in Eq. (8), which is defined as being proportional to the ratio between the bubble growth rate and the liquid shear velocity. Thus, an inaccurate bubble growth rate may affect the estimation of convective heat transfer enhancement factor, leading to an overprediction of wall temperature at $P = 17$ bar.

5. Conclusion

In order to assess the influence of boundary conditions on R134a flow boiling, tests were conducted on KIMOF facility using a 10 mm-diameter vertical tube. These experiments, along with other public water boiling experiments and n-Perfluorohexane boiling experiments in pipes or rectangle channels, provided additional data for assessing the new wall boiling heat transfer model. Additionally, the effects of various boundary conditions such as mass flux, pressure, and inlet subcooling on the wall superheat were also investigated. The main conclusions are as follows.

(1) The new wall boiling heat transfer model shows great potential in boiling calculations, not only for various fluids such as R134a, water, and n-Perfluorohexane but also in different geometries, including vertical pipes and rectangular channels.
(2) For R134a boiling, under the boundary conditions of $P = 11$–17 bar, $G = 1000$–2000 kg/(m^2·s), $q_w = 80$–220 kW/m^2, $\Delta T_{in,sub} = 19$–38 K, the mean relative error between the experimental and calculated wall superheat is ±31.5 %.
(3) Pressure significantly influences the model accuracy. Specifically, the new model tends to overpredict wall temperature at relatively

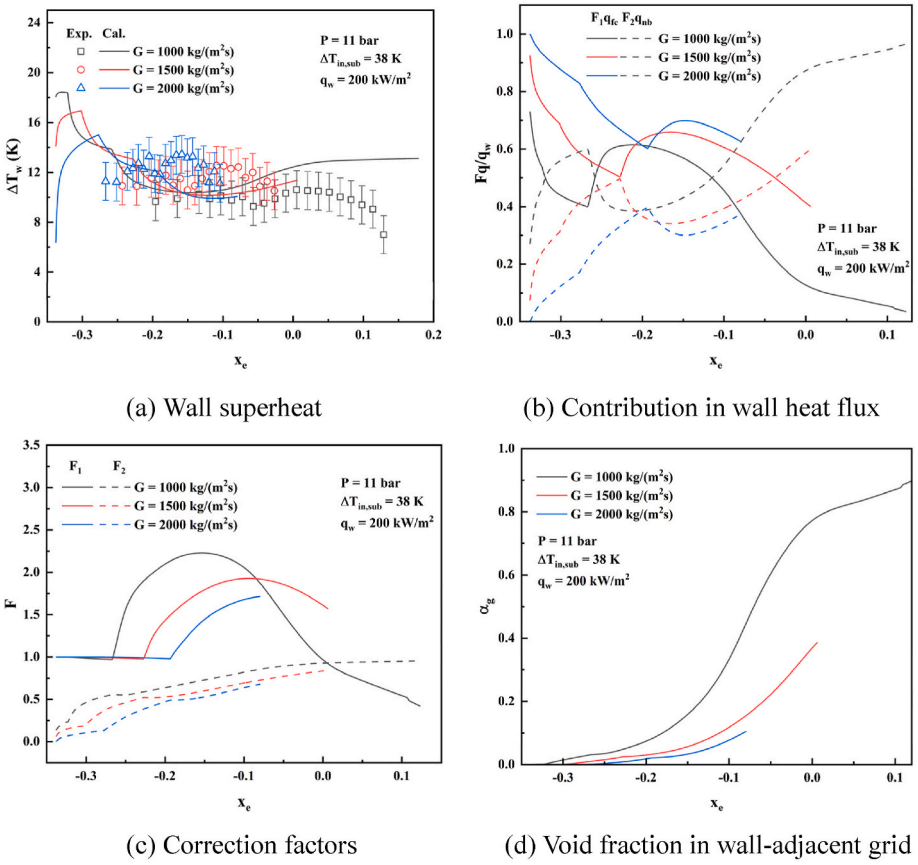

Fig. 13. Analysis of the impacts of different mass flux.

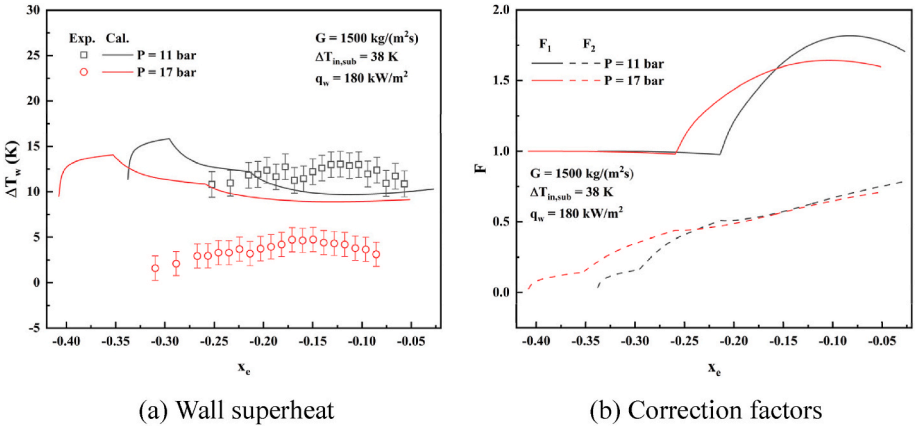

Fig. 14. Analysis of the impacts of different pressure.

higher pressures. The results suggest that the new model lacks consideration of pressure effects when calculating bubble growth rate and bubble size, leading to inaccuracies in both factor F_2 and factor F_B. Improving the treatment of pressure effects can be a potential direction for future improvements.

(4) The new wall boiling model reasonably predicts wall superheat under different mass flow rates, demonstrating its applicability in various flow rate conditions. However, the current model ignores the effects of bubble departure and sliding in the enhancement factor F_B, which could disturb the thermal boundary layer, thereby enhancing convective heat transfer, and should be sensitive to flow rate. This limitation suggests that considering departure and sliding effects into F_B could improve model accuracy in predicting heat transfer.

CRediT authorship contribution statement

Xiang Zhang: Writing – original draft, Validation, Software, Methodology, Investigation, Formal analysis. **Jie Wan:** Writing – original draft, Validation, Investigation, Data curation. **Nikolai Rensch:** Investigation, Data curation. **Xu Cheng:** Writing – review & editing, Supervision, Resources, Methodology, Conceptualization.

Declaration of competing interest

The authors declare that they have no known competing financial interests or personal relationships that could have appeared to influence the work reported in this paper.

Acknowledgements

The authors would like to thank the China Scholarship Council (CSC) and the German Academic Exchange Service (DAAD) for providing the financial support.

Data availability

Data will be made available on request.

References

ANSYS-Fluent, 2011. Ansys Fluent Theory Guide. Ansys Inc, USA, pp. 724–746.
Bartolemei, G.G., Brantov, V.G., Molochnikov, Y.S., Kharitonov, Y.V., Solodikk, V.A., Batashove, G.N., Mikhailov, V.N., 1982. An experimental investigation of true volumetric vapor content with subcooled boiling in tubes. Therm. Eng. 29, 132–135.
Bartolemei, G.G., Chanturiya, V.M., 1967. Experimental study of true void fraction when boiling subcooled water in vertical tubes. Therm. Eng. 14, 123–128.
Braz Filho, F.A., Ribeiro, G.B., Caldeira, A.D., 2016. Prediction of subcooled flow boiling characteristics using two-fluid Eulerian CFD model. Nucl. Eng. Des. 308, 30–37.
Chen, J.C., 1966. Correlation for boiling heat transfer to saturated fluids in convective flow. Ind. Eng. Chem. Process Des. Dev. 5, 322–329.
Dahariya, S., Betz, A.R., 2019. High-pressure pool boiling: mechanisms for heat transfer enhancement and comparison to existing models. Int. J. Heat Mass Tran. 141, 696–706.
de Bertodano, M.A.L., 1992. Turbulent Bubbly Two-phase Flow in a Triangular Duct. Rensselaer Polytechnic Institute.
Devahdhanush, V.S., Mudawar, I., Nahra, H.K., Balasubramaniam, R., Hasan, M.M., Mackey, J.R., 2022. Experimental heat transfer results and flow visualization of vertical upflow boiling in Earth gravity with subcooled inlet conditions – in preparation for experiments onboard the International Space Station. Int. J. Heat Mass Tran. 188, 122603.
Feldman, A., Marvillet, C., Lebouche, M., 2000. Nucleate and convective boiling in plate fin heat exchangers. Int. J. Heat Mass Tran. 43, 3433–3442.
Forster, H., Zuber, N., 1955. Dynamics of vapor bubbles and boiling heat transfer. AIChE J. 1, 531–535.
Gilman, L.A., 2014. Development of a General Purpose Subgrid Wall Boiling Model from Improved Physical Understanding for Use in Computational Fluid Dynamics. Institute of Technology, Massachusetts, USA.
Ishii, M., 1990. Two-fluid model for two-phase flow. Multiphas. Sci. Technol. 5.
Khoshnevis, A., Sarchami, A., Ashgriz, N., 2018. Effect of nucleation bubble departure diameter and frequency on modeling subcooled flow boiling in an annular flow. Appl. Therm. Eng. 135, 280–288.
Köckert, L., Badea, A.F., Cheng, X., Yu, D., Klingel, D., 2021. Studies on post-dryout heat transfer in R-134a vertical flow. Int. J Adv. Nucl. React. Design Technol. 3, 44–53.
Lavieville, J., Quemerais, E., Mimouni, S., Boucker, M., Mechitoua, N., 2005. NEPTUNE CFD V1.0 Theory Manual. EDF, France.
Lemmert, M., Chawla, J., 1977. Influence of Flow Velocity on Surface Boiling Heat Transfer Coefficient. Academic Press and Hemisphere, New York and Washington D. C.
Liang, G., Zhang, Z., Bu, S., Liu, H., Chen, D., 2023. Numerical study of thermal-hydraulic and structural parameters effects on CHF in subcooled forced convection flow during external reactor vessel cooling. Prog. Nucl. Energy 165, 104939.
Lin, Y.-C., Zhao, Y., Ishii, M., Schlegel, J.P., Hogan, K.J., Buchanan, Jr J.R., 2021. Assessment of nucleation boiling models and improvement by the chen correlation for two-fluid model CFD. Int. J. Heat Mass Tran. 175, 121363.
Liu, K., Wang, M., Gan, F., Tian, W., Qiu, S., Su, G.H., 2021. Numerical investigation of flow and heat transfer characteristics in plate-type fuel channels of IAEA MTR based on OpenFOAM. Prog. Nucl. Energy 141, 103963.
Moraga, F., Bonetto, F., Lahey, R., 1999. Lateral forces on spheres in turbulent uniform shear flow. Int. J. Multiphas. Flow 25, 1321–1372.
Orian, G., Jelinek, M., Levy, A., 2010. Flow boiling of binary solution in horizontal tube. Energy 35, 35–44.
Ranz, W.E., 1952. Evaporation from Drops-I and-II. Chem. Eng. Prog. 48 (141–146), 173–180.
Sateesh, G., Das, S.K., Balakrishnan, A.R., 2005. Analysis of pool boiling heat transfer: effect of bubbles sliding on the heating surface. Int. J. Heat Mass Tran. 48, 1543–1553.
Sato, Y., Sekoguchi, K., 1975. Liquid velocity distribution in two-phase bubble flow. Int. J. Multiphas. Flow 2, 79–95.
Shi, J., Zhang, R., Zhu, Z., Ren, T., Yan, C., 2020. A modified wall boiling model considering sliding bubbles based on the RPI wall boiling model. Int. J. Heat Mass Tran. 154, 119776.
Utaka, Y., Kashiwabara, Y., Ozaki, M., Chen, Z., 2014. Heat transfer characteristics based on microlayer structure in nucleate pool boiling for water and ethanol. Int. J. Heat Mass Tran. 68, 479–488.
Wang, M., Li, L., Liu, K., Zhang, J., Tian, W., Qiu, S., Su, G., 2022. Development of subcooled wall boiling model considering bubble sliding in narrow rectangular channel. Int. J. Therm. Sci. 181, 107787.
Yang, G., Zhang, W., Binama, M., Li, Q., Cai, W., 2023. Review on bubble dynamic of subcooled flow boiling-part b: behavior and models. Int. J. Therm. Sci. 184, 108026.
Zhang, R., Cong, T., Tian, W., Qiu, S., Su, G., 2015. Effects of turbulence models on forced convection subcooled boiling in vertical pipe. Ann. Nucl. Energy 80, 293–302.
Zhang, X., Cheng, X., Liu, W., 2024. Development of a new semi-mechanistic wall boiling heat transfer model for CFD methodology focusing on macroscopic parameters. Int. J. Heat Mass Tran. 224, 125309.
Zhou, P., Hua, S., Gao, C., Sun, D., Huang, R., 2021. A mechanistic model for wall heat flux partitioning based on bubble dynamics during subcooled flow boiling. Int. J. Heat Mass Tran. 174, 121295.